Corrosion behaviour of single layered ZrN_xO_y thin films in artificial sweat solutions

E. Ariza[1*], L. A. Rocha[1,2], S.C. Ferreira[1], F. Vaz[3], L. Cunha[4], P. Carvalho[3], L. Rebouta[3], E. Alves[5], Ph. Goudeau[6], J. P. Rivière[6]

[1] Research Centre on Interfaces and Surfaces Performance, Campus Azurém, 4800-058 Guimarães, Portugal
[2] Universidade do Minho, Dept. Engª. Mecânica, Campus Azurém, 4800-058 Guimarães, Portugal
[3]Universidade do Minho, Dept. Física, Campus Azurém, 4800-058 Guimarães, Portugal
[4]Universidade do Minho, Dept. Física, Campus de Gualtar, 4710-057 Braga, Portugal
[5]ITN, Departamento de Física, E.N.10, 2685 Sacavém, Portugal
[6]Laboratoire de Métallurgie Physique, Université de Poitiers, 86960 Futuroscope, France

Applications of coloured thin films can be found on the production of high-quality consumer products, such as eyeglass frames, wristwatch casings and wristbands. These components should possess scratch and corrosion resistant surfaces through the desired lifetime. Recently, metal oxynitrides, MeN_xO_y (Me = early transition metal) were proposed for decorative applications. In these materials, variations on the amount of oxygen allow the film properties to be tailored, originating a wide range of colours. Additionally, these materials should also fulfil the wear and corrosion requirements above referred.
In the present work the corrosion behaviour of single layered zirconium oxynitride, ZrN_xO_y films, immersed in artificial sweat solutions, is described. Films were produced by rf reactive magnetron sputtering at a constant substrate temperature of 300 ºC, from a pure Zr target. The main processing variable was the flow rate of reactive. The corrosion resistance was evaluated by potentiodynamic polarisation tests and Electrochemical Impedance Spectroscopy (EIS) at different immersion times, at room temperature.

The corrosion resistance of the films is strongly affected by the O/N ratio. A slight tendency to improving the corrosion resistance of the films was found with the increasing in the atomic fraction of oxygen. Nevertheless, pitting was found in all samples. However, the amount of pits seems to be strongly dependent not only on the composition of the film, but also on the processing-induced defects distribution.

Keywords: Decorative Films; EIS; thin films

1. Introduction

In the field of coating technology, nitrides and oxynitrides represent a group of materials with increasing technological importance. Due to their great wear resistance, they are used as hard-coating to increase the lifetime of mechanical components such as cutting tools and dies. In electronic industry, because of their electronic properties, they are employed as electrical contacts; and for decorative purposes, they are also used due to their wide range of colours. As decorative films, these materials possess a high potential for being applied in high-quality consumer products, such as eyeglass frames, wristwatch casings and wristbands. In fact, while enhancing the appearance of the pieces by lending attractive colorations to their surfaces, these films are supposed to provide simultaneously scratch-resistance and improved corrosion resistance [1].

In the last few years, a new class of materials is reaching significance for these decorative applications, the so-called metal oxynitrides, MeN_xO_y (Me = early transition metal) [2-3]. Their importance results from the existence of oxygen that allows the tailoring of film properties between those of "pure" covalent metal nitride and those of the correspondent mainly ionic oxides. Recent works suggest that the performance of these oxynitrides depends not only on the deposition method but also on both the concentration and distribution of the nitrogen atoms incorporated into the matrix [2-5].

In spite of the published works on thin films of metallic nitrides and oxides over the last years [6], the study of the metal oxynitrides is insufficient and the understanding of the fundamental mechanism to explain both structural and mechanical behaviour is yet limited. In addition, no studies known exist about of corrosion behaviour and degradation mechanisms that take place in these films when they are in contact with aggressive environments. In this work the electrochemical properties of thin ZrN_xO_y films in contact with artificial sweat solutions are explore. Particular importance is given to the study of corrosion mechanisms associated to the variations in the oxygen/nitrogen ratio.

2. Experimental details

The ZrN_xO_y single layer films were produced by reactive rf magnetron sputtering from a high purity Zr target onto polished high-speed steel (AISI M2) substrates. Depositions were carried out under an Ar/N_2+O_2 atmosphere in an Alcatel SCM650 apparatus. The pressure in the deposition chamber was about 10^{-4} Pa and rose to values around $5x10^{-1}$ Pa during depositions. Films were prepared with variation of the gas mixture (N_2+O_2), using constant values of temperature (300 ºC) and bias voltage of – 50 V. Reactive gas fluxes varied from 3.3 to 6.3 sccm, with a partial pressure ranging from 0.02 to 0.05 Pa. The working gas flow (Ar) was kept constant at 100 sccm. A pure Zr adhesion layer with a thickness of about 0.30 μm was deposited in each sample in order to improve the film adhesion.

The atomic composition of the films was measured by Rutherford backscattering spectrometry (RBS). An average number of 5 ball cratering experiments were carried out in each sample in order to determine its thickness. The morphology of the films was studied by SEM and AFM analyses. Image analyse of images obtained by Optical Microscopy was also used to quantify the superficial defects of the samples, which were determined calculating the ratio between the defective area and the total analyzed area. The surface roughness of the samples was calculated from 5μm x 5 μm line scans by AFM analyses.

The corrosion behaviour was evaluated by potentiodynamic polarization and electrochemical impedance spectroscopy (EIS) measurements. Previously to corrosion tests the samples were ultrasonically cleaned in ethanol during 15 minutes, then in distilled water during 10 minutes and finally dried. The electrochemical test were performed at room

temperature in an artificial sweat solution (pH = 4.5), containing 7.5 $g.l^{-1}$ NaCl; 1.2 $g.l^{-1}$ KCl; 1 $g.l^{-1}$ CH_4N_2O (urea) and 1 $ml.l^{-1}$ $C_3H_6O_3$ (lactic acid). An electrochemical cell constituted by a standard three electrode arrangement was used for the electrochemical test. The counter electrode was a platinum sheet with an area of 1 cm^2 and a saturated calomel electrode (SCE) was used as reference. The area of the work electrode was set in 0.173 cm^2. A PGP201 Potentiostat/Galvanostat (Radiometer Denmark), controlled by the VoltaMaster software, was used to carry out the polarization measurements, while a Voltalab PGZ100 Potentiostat (Radiometer Analytical), controlled by the VoltaMaster-4 software, was used for the EIS measurements. Prior to polarization tests the open circuit potential (OCP) was monitored during 3600 s, after which the samples were anodically polarised from -800 mV to 2000 mV at a scan rate of 2 $mV.s^{-1}$. The EIS measurements, carried out at increased immersion times (1, 2 and 3 hours, as well as 1, 2 and 3 days) were performed in the frequency range from 100 KHz to 5 mHz, with an AC sine wave amplitude of 10 mV applied to the electrode at its corrosion potential. For EIS data simulation the ZView2 software was used.

After potentiodynamic polarization tests an examination and evaluation of pitting corrosion was carried out in according to standard ASTM G-46 [7]. Three main parameters were determined: the pit density (number of pits per unit area), the pits size (average of pit size) and the pit depth (average of pit depth). The pit density was calculated through image analysis of SEM images at a magnification of 28x, in an area of 12.47 mm^2. These same images were used to determine the average of the size pit. Finally, pith depth was calculated by sectioning vertically through the pre-selected pits. The polished surfaces containing the pits cross section were observed and analysing by an optical microscopy with a calibrated eyepiece.

3. Results and Discussion

3.1. Morphological, chemical and structural characterization

In Fig. 1(a), a representative SEM micrograph of the cross-section of the ZrN_xO_y films is shown. As it can be observed, the films show a typical columnar microstructure formed by slight columnar grains with compactly fibrous morphology. Also, as shown in Fig. 1(b), the grains present a superficial dome-rounded shape, characteristic of this kind of films.

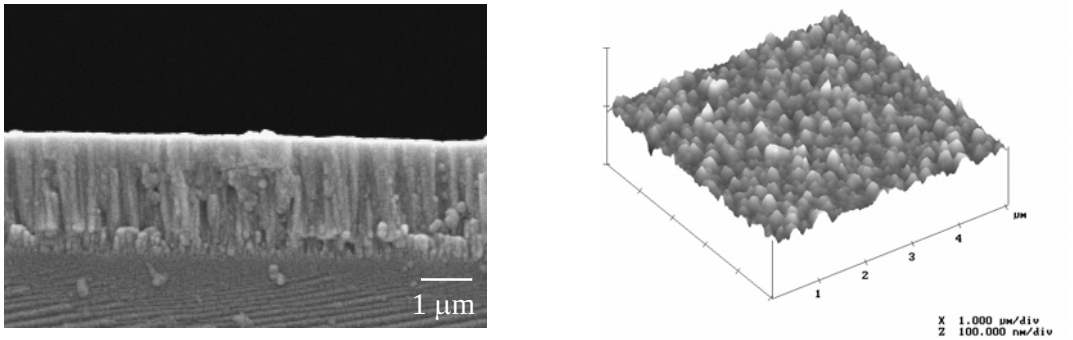

(a) **(b)**

Figure 1. *SEM micrograph of the cross-section (a) and AFM image of the surface of a typical sample from the ZrN_xO_y system(b).*

In Table I the chemical composition, thickness, surface roughness and density of defects are presented. The oxygen fraction in each sample was determined by the ratio between the

oxygen content and the sum of both oxygen and nitrogen contents: $fO_2 = C_O/(C_O+C_N)$. As it can be seen, films with low oxygen fractions show lower values of surface roughness. In contrast, a higher surface roughness was found to be characteristic of the highest oxygen fractions. In these last samples, an increase in the oxygen fraction, also conduce to a slight decrease in the roughness, as it can be confirmed by the observation of the AFM images.

Table I. *Chemical and morphological characterisation of ZrN_xO_y films*

Sample	fO_2	Zr (at. %)	N (at. %)	O (at. %)	Thickness (μm)	R_a (nm)	Defects (%)
ZrN	0	50	50	0	4.4± 0.1	3.0	8.5
$ZrN_{1.14}O_{.14}$	0.11	44	50	6	2.3 ± 0.2	3.6	3.2
$ZrN_{.91}O_{.26}$	0.22	46	42	12	3.2 ± 0.1	3.2	8.4
$ZrN_{.87}O_{.30}$	0.26	46	40	14	3.0 ± 0.2	6.0	7.6
$ZrN_{.87}O_{.36}$	0.29	45	39	16	3.2 ± 0.2	5.0	5.1
$ZrN_{.86}O_{.41}$	0.32	44	38	18	1.3 ± 0.1	4.7	4.3
$ZrNO_{.50}$	0.33	40	40	20	2.0 ± 0.3	3.6	3.7
ZrO_2	1	34	0	66	2.16± 0.2		2.8

GIXRD patterns obtained for the ZrN_xO_y films showed diffraction patterns corresponding to a fcc ZrN phase. No diffraction peaks from oxide phases were observed. With the increasing in the oxygen amount, it is to admit that oxygen might be in grain boundaries and/or within oxide amorphous phases. Furthermore, the ZrN grain size seems to decrease with increasing oxygen fraction and the very broad peak around $2\theta = 30^\circ$ is an indication of either the amorphization of the ZrN phase induced by the oxygen inclusion or the formation of an amorphous oxide phase.

3.2. Corrosion behaviour

3.2.1. Potentiodynamic Polarisation

In Fig. 2 an overlap of the potentiodynamic polarization curves obtained for some representative ZrN_xO_y films is showed. In order to compare the behaviour of the samples, the polarization curves of the steel substrate and of pure Zr are also plotted.

Results of potentiodynamic polarization measurements show that the corrosion resistance of the M2 steel, used as substrate, is visibly improved by the deposited films. In contrast, the graph shows that the pure Zr film, although possessing a lower pitting potential, presents a passive current density two orders of magnitude lower that of the ceramic, suggesting a superior corrosion resistance for this sample. Concerning to the ZrN_xO_y films, no significant differences between samples are evidenced. As can be seen in Fig. 4., the only exception occurs with the film with a $fO_2 = 0.32$, which appear to present a slightly higher pitting potential and a passive current density lower that of the other ZrN_xO_y films; this being indicative of a better corrosion resistance when compared with the other ZrN_xO_y films. In general terms, a well defined large potential independent region, indicative of a passive plateau, is exhibited by all samples.

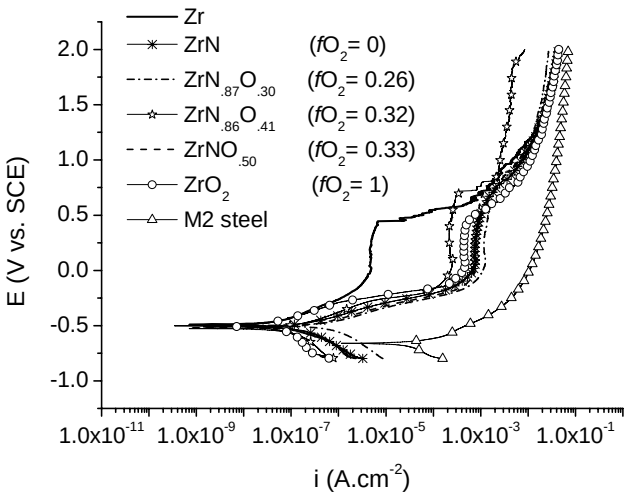

Figure 2. *Anodic polarisation curves obtained for ZrN_xO_y prepared with the same N/O ratio and variation of the bias voltage.*

3.2.2. Evaluation of pitting

ASTM standard G46 classifies pits in terms of density, size and depth (referred as A, B and C, respectively) and establishes standard charts which correlates those parameters. Each parameter (A, B, or C) is then classified in five grades (1-5), with increasing extent of pitting. A and B parameters are related to the extent of pitting at the surface of the metal, while C refers to the depth of the attack.

In Fig. 3 representative micrographs referring to A, B, and C parameters are presented. As it can be seen, pitting may be classified as A-5, B-1, C-1, for all samples. This means that all films, except the Zr film, showed a very high pit density (A), superior to $5x10^5$ pits.m^{-2}. However, the average pit size at the surface (B) was found to be very low (< 0.5 mm^2), and the average pit depth was also found to be very low (< 0.4 mm). In all films, the pit shape showed a round opening. The small values of these last parameters, suppose a little level of penetration of electrolyte down to the substrate through the film (film thickness between 1.3 and 4.4 μm), which is also in accordance with the low corrosion current density (i_{corr}), obtained from potentiodynamic polarisation curves for all films. Nevertheless, pit density appears to be correlated with i_{corr}, as shown in Fig. 4. As plotted in the graph, the corrosion rate for all films is very low (< 0.4 μA.cm^{-2}). The average pit size and pit depth are also indicated in the graph.

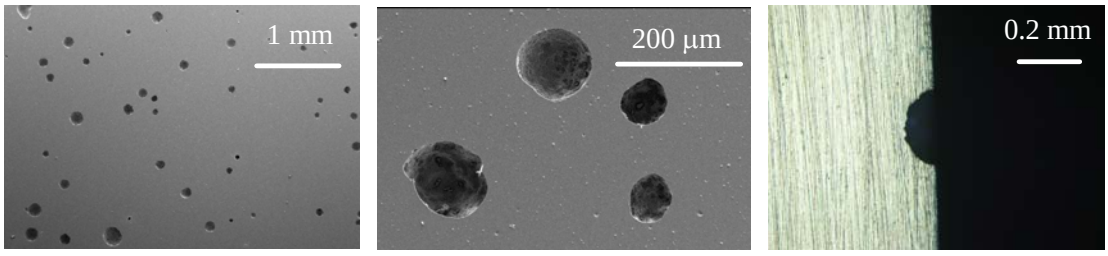

(a) **(b)** **(c)**

Figure 3. *Representative micrographs referring to pit density-A (a), pit size-B (b) and pit depth-C (c) linked to the standard rating charts for the evaluation of the pitting corrosion.*

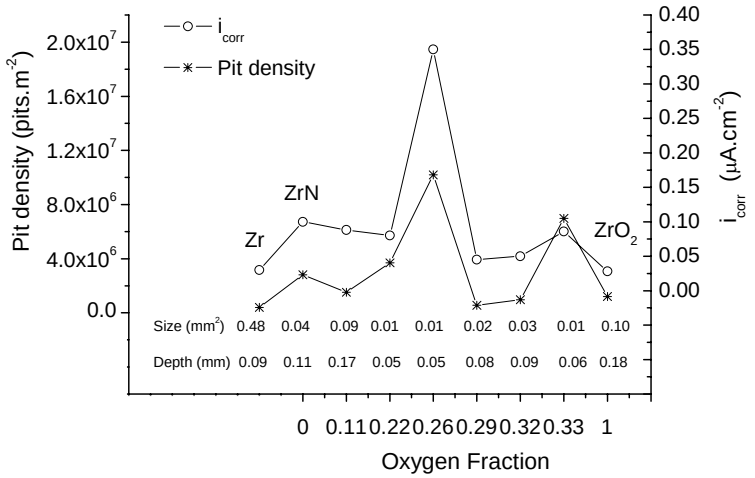

Figure 4*. Influence of the atomic fraction of oxygen on the i_{corr} and pit density of the Pure Zr and ZrN_xO_y films. The size pit and depth pit are also presented.*

3.2.3. Electrochemical Impedance Spectroscopy

In Fig. 5, the Bode impedance (a) and Bode phase (b) plots obtained for some ZrN_xO_y representative films at 2 hours of immersion are presented. In Fig. 6, the same plots obtained at 3 days of immersion are shown. In both cases the behaviour for the pure Zr film is also presented.

The comparison of the graphs presented in Fig. 5a and 6a shows that the AC impedance decreases as immersion time increases, for all samples. This is an indication of a degradation of the corrosion resistance of the film due to the prolonged contact with the aggressive medium. On the other hand, an analysis of the time constants (phase angle maximums) presented in the graph Bode phase plots (Fig. 5b and 6b) can contribute to elucidate the coating properties and/or detect the presence or absence of defects or discontinuities along the different interfaces constituting the coating [8-10]. In fact, the Bode phase plot in Fig. 5b, shows a single time constant with a high phase angle, in the broad low and middle frequency range, for ZrN, ZrN_xO_y, and Zr films, indicating the good corrosion resistance of these films at early stages of the immersion. Actually, this short period of immersion is insufficient to reveals any degradation of the substrate via surface defects. In fact, it is well known that surface defects can act as preferential routes for the penetration of the solution through the coating [11,12]. In case of ZrO_2 film, as can be seen in Fig. 5b and 6b, the two time constants, are revealed at short and large immersion times. However, the first time constant at high frequency ranges shows a high phase angle that remains almost unaffected during the immersion time (see Fig. 6b), this being indicative of a good capacitive behaviour of the solution/film interface, when compared with the other films.

On the other hand, the Bode plot after 3 days of immersion (Fig. 6b) can supply important information regarding the progress of the degradation process of the films. In fact, with the exception of the Zr film, which tend to keep in a wide frequency range a high phase angle, in confirmation of the good capacitive response of this film, all other films reveals now two well defined time constants. In case of ZrN and ZrN_xO_y films, these time constants are located at low and middle frequency ranges. The time constant at middle frequency may express the adhesion layer/film/solution interface response, which is better for the ZrN film

and worst for the ZrN_xO_y film. The second time constant in the low frequency region is related with the substrate/adhesion layer/film interface response and might be interpreted as being due to the fact that the electrolyte had entered in contact with the substrate, owing to discontinuities and defects existing in the film.

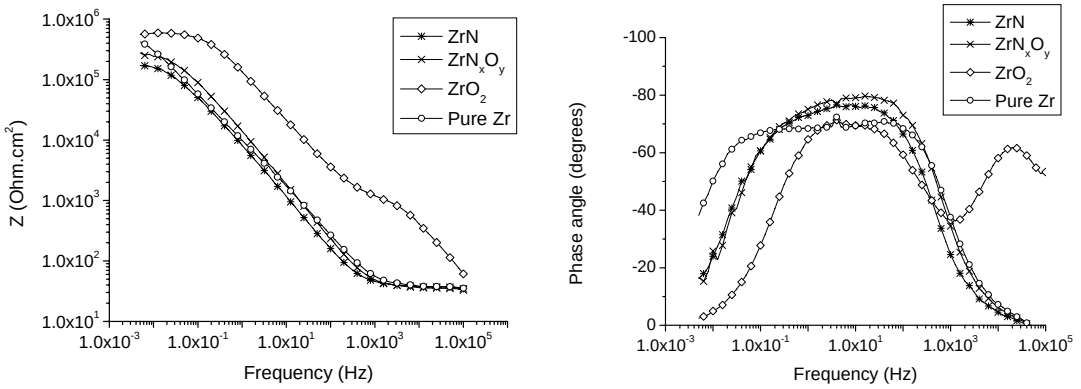

a) **b)**

Figure 5. *Bode impedance (a) and Bode phase (b) plots obtained in ZrN, ZrN_xO_y, ZrO_2 and Zr films after 2 hours of immersion.*

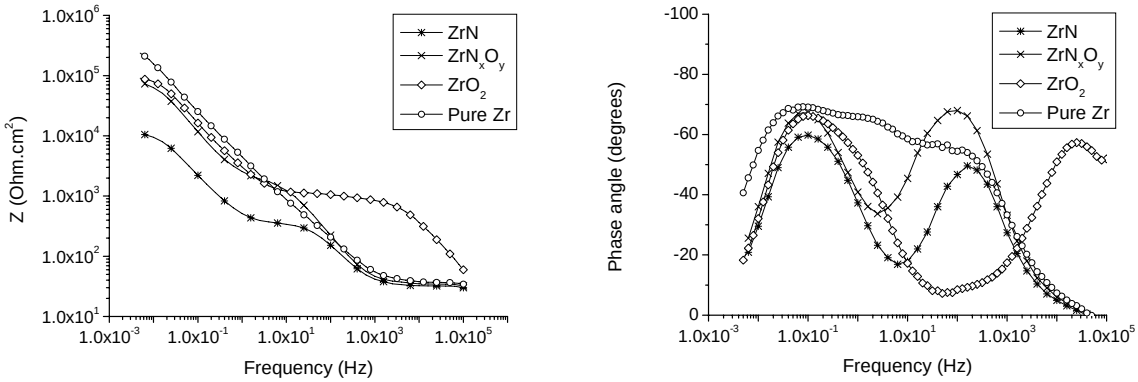

a) **b)**

Figure 6. *Bode impedance (a) and Bode phase (b) plots obtained in ZrN, ZrN_xO_y, ZrO_2 and Zr films after 3 days of immersion.*

It is generally assumed that the electric elements of an equivalent circuit are well correlated with the corrosion properties of the system [13]. An equivalent circuit, composed by the electrolyte resistance (R_e) in series with two pair of elements in parallel was proposed in this work. The first pair, which represents the dielectric properties of the film, is composed by the film capacitance (C_f) and by the film polarisation resistance (R_{pf}). The second pair related with the processes occurring in the electrolyte/substrate interface, is composed by the same electric elements: the double layer capacitance (C_{dl}) and the polarisation resistance of the substrate (R_{ps}). It should be referred that a good agreement between the fitted and the experimental data was obtained.

Fig. 7 shows the evolution of the polarization resistance (R_p) with the immersion time, as a function of the fO_2. For comparison, the corrosion current density (i_{corr}) for all samples is also presented. The polarisation (R_p) is an electrochemical parameter, which is inversely

proportional to the corrosion rate; this parameter was calculated by the sum of R_{ps} and R_{pf}, deduced by the EIS data simulation, in accordance to the method described by Liu et al. [14]. As it can be observed in Fig. 7, all samples show very low i_{corr} values. A slight general trend for an improvement of the corrosion resistance with the increase of the oxygen content of the oxynitrides can be inferred from i_{corr} and R_p values plotted in the graph, suggesting better corrosion behaviour of the ZrO_2 film. It should be remarked the behaviour of the pure Zr film because it, in opposition at the other films, appears to remain a very high R_p even after being in contact with the artificial sweat solution during 3 days.

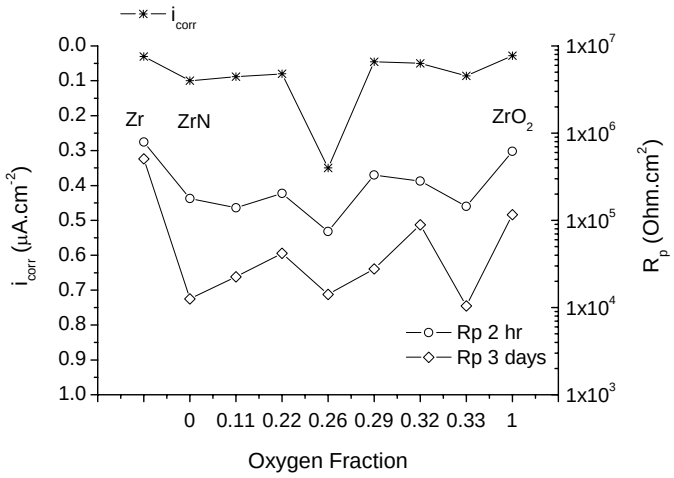

Figure 7. *Influence of the atomic fraction of oxygen on the i_{corr} and polarisation resistance (R_p) of the ZrN_xO_y films. For comparison, the i_{corr} and R_p for pure Zr is also plotted.*

In the same way, as it can be seen in Fig. 8a, a small tendency for an improvement in the R_p, with the decreasing of the film thickness and the surface defects can be observed. However, is important to remark that in the range $0.22 < fO_2 < 0.33$ the R_p appears to be quite sensitive to small variations of fO_2. As discussed elsewhere [15], a complex group of factors are expected to play a role concerning this behaviour. In fact variations in chemical composition, grain size, texture, amorphization of the ZrN structure, and/or distribution of the oxygen in the structure might also influence the degradation of the material.

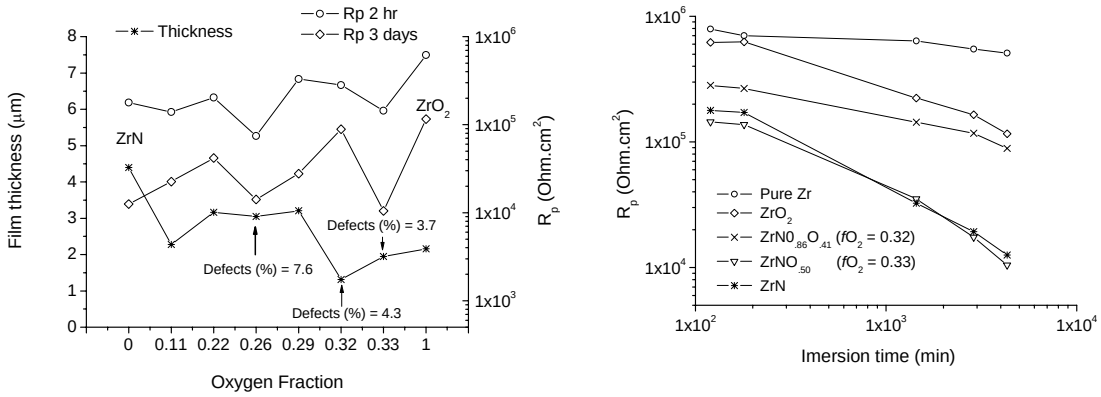

a) **b)**

Figure 8. *(a) Evolution of the polarisation resistance (R_p) and the film thickness with the atomic fraction of O_2. (b) Evolution of polarisation resistance (R_p) with the immersion time.*

As already showed in the Bode impedance plots (Figs. 5a and 6a), the corrosion resistance of the films diminish drastically with the increase in the immersion time. This phenomena is clearly evidenced in Fig. 8b, which shows the evolution of R_p with the immersion time (for convenience, only the ZrN_xO_y curves with fO_2=0.32 and fO_2=0.33 are plotted in the graph). The ZrN film and the ZrN_xO_y film with fO_2=0.33 appear to be the most sensitive to this detrimental effect of the immersion time on the film corrosion protection character. In contrast, the polarization resistance of the ZrO_2 film approaches that of the Zr film during the first hours of immersion, but then decrease to values near that of the ZrN_xO_y film with fO_2=0.32. The polarisation resistance of these last three films remains relatively stable throughout the 3 immersion days, when compared with the others samples, this being an indication of a better stability of the films when in contact with the artificial sweat solution.

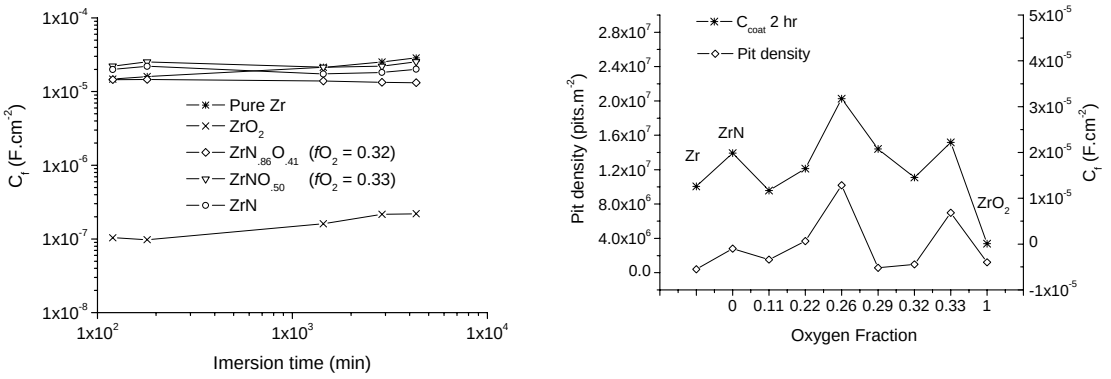

a) **b)**

Figure 9. *(a) Evolution of the film capacitance (C_f) with the immersion time , (b) variation of the films capacitance and the pit density with the oxygen fraction, obtained for the ZrN, ZrN_xO_y, ZrO_2 and pure Zr films.*

The dielectric characteristics of the film may be described by the film capacitance (C_f). In general terms, a film performs a better character protector when possess a low capacitance value (low dielectric constant). Fig. 9a, shows the variation of the film capacitance with the immersion time. As it can be seen, C_f remains relatively constant along of immersion time in all films. However, a great difference between C_f of ZrO_2 and the other films was founded. In fact, the low capacitance evidenced by the ZrO_2 film when compared to that of the others may be considered as an indication of the superior insulation character of this film. On the other hand, as shown in Fig. 9b, a relation between film capacitance and the pit density was found. Thus, when the capacitance of film is elevated (see ZrN film, and ZrN_xO_y films with fO_2=0.26. and fO_2=0.33) the quality of film decreases, resulting in a higher quantity of pits and therefore in a higher corrosion rate (see Fig.4).

4. Conclusions

The degradation of the samples in artificial sweat solution was investigated by EIS technique and complemented with potentiodynamic polarisation tests.

The films obtained by rf reactive magnetron sputtering promote a clearly improvement of the corrosion resistance of the M2 steel, used as substrate. In these films, when the O/N ratio is increasing during processing, the corrosion resistance tend to be slightly improved. However, the corrosion behaviour of the coating system appears to be governed by a complex

interrelated ensemble of chemical, structural, textural, morphological and electronic characteristics of the films. Concerning to the pure Zr films, its superior corrosion resistance was evidenced, when compared to the ZrN, ZrN_xO_y and ZrO_2 coating systems. Also, a better isolated behaviour of the ZrO_2 films, when compared to the other systems was detected. In practice, it appears to possess a higher corrosion resistance than the ZrN and ZrN_xO_y films, due to the cumulative contribution of the good impedance characteristics of the film/solution, film/adhesion layer and adhesion layer/substrate interfaces.

Acknowledgements

The authors gratefully acknowledge the financial support of the European Union through the NMP3-CT-2003-505948 project "HARDECOAT". Acknowledgments also to Portuguese FCT institution by the contract SFRH/BPD/5518/2001 and by the project nº POCTI/CTM/380860/2001 co-financed by European community fund FEDER.

References

1. E. Budke, J. Krempel-Hesse, H. Maidhof, H. Schussler, Surf. Coat. Technol., **112** (1999) 108.
2. F. Vaz, P. Cerqueira, L. Rebouta, S. M. C. Nascimento, E. Alves, Ph. Goudeau, J. P. Rivière, Surf. Coat. Technol., **174-175** (2003) 197.
3. E. Alves, A. Ramos, N. Barradas, F. Vaz, P. Cerqueira, L. Rebouta, U. Kreissig, Surf. Coat. Technol. (in print).
4. M. Bhat, L. K. Han, D. Wristers, J. Yan, D. L. Kwong, and J. Fulford, Appl. Phys. Lett., **66** (1995) 1225.
5. W. L. Hill, E. M. Vogel, V. Misra, P. K. McLarty, and J. J. Wortman, IEEE Trans. Electron Devices, **43** (1996) 15.
6. R. Fraunchy, Surface Science Reports, **38** (2000) 195.
7. ASTM G 46-94, "Standard Practice for Examination and Evaluation of Pitting Corrosion", Annual Book of ASTM Standars, Section three, Vol. 03.02, ASTM international, Philadelphia, P.A (2002)
8. C.H. Tsai and F. Mansfeld, Corrosion, **49** (1993) 726.
9. M.C. Garcia-A., M.L. Escudero, J.L. Gonzalez-Carrasco, J. Chão, Biomaterials, **21** (2000) 79.
10. I. García, J.J. de Damborenea, Corrosion Science, **40** (1998) 1411.
11. L.A. Rocha, E. Ariza, J. Ferreira, F. Vaz, E. Ribeiro, L. Rebouta, E. Alves, A.R. Ramos, Ph. Goudeau, J.P. Rivière, Surf. Coat. Technol., **180-181** (2004)158.
12. C. Liu, Q. Bi, A. Matthews, Corrosion Sci., **43** (2001) 1953.
13. F. Mansfed, Electrochim. Acta, **38** (1993) 1891.
14. C. Liu, A. Leyland, Q. Bi, A. Matthews, Surf. Coat. Technol., **141** (2001) 164.
15. E. Ariza, L. A. Rocha, F. Vaz, L. Cunha, S.C. Ferreira, P. Carvalho, L. Rebouta, E. Alves, Ph. Goudeau, J. P. Rivière, Surface and Coatings Technology (Accepted).